

# SOLVING SCHUBERT PROBLEMS WITH LITTLEWOOD-RICHARDSON HOMOTOPIES

FRANK SOTTILE, RAVI VAKIL, AND JAN VERSCHELDE

**ABSTRACT.** We present a new numerical homotopy continuation algorithm for finding all solutions to Schubert problems on Grassmannians. This Littlewood-Richardson homotopy is based on Vakil's geometric proof of the Littlewood-Richardson rule. Its start solutions are given by linear equations and they are tracked through a sequence of homotopies encoded by certain checker configurations to find the solutions to a given Schubert problem. For generic Schubert problems the number of paths tracked is optimal. The Littlewood-Richardson homotopy algorithm is implemented using the path trackers of the software package PHCpack.

## 1. INTRODUCTION

The Schubert calculus is concerned with geometric problems of the form: Determine the  $k$ -dimensional linear subspaces of  $\mathbb{C}^n$  that meet a collection of fixed linear subspaces in specified dimensions. For example, what are the three-dimensional linear subspaces of  $\mathbb{C}^7$  that meet each of 12 general four-dimensional linear subspaces in at least a line? (There are 462 [14].) The traditional goal is to count the number of solutions and the method of choice for this enumeration is the Littlewood-Richardson rule, which comes from combinatorics and representation theory [4]. Recently, Vakil gave a geometric proof of this rule [20] through explicit specializations organized by a combinatorial checkers game.

Interest has grown in computing the solutions to actual Schubert problems. One motivation has been the experimental study of reality in the Schubert calculus [6, 16, 17, 19]. A proof of Pieri's rule (a special case of the Littlewood-Richardson rule) using geometric specializations [18] led to the Pieri homotopy for solving special Schubert problems [7]. This was implemented and refined [8, 11, 22, 23, 24], and has been used to address a problem in pure mathematics [9]. Another motivation is the output pole placement problem in linear systems control [1, 2, 3, 13, 23].

We present the Littlewood-Richardson homotopy, which is a numerical homotopy algorithm for finding all solutions to any Schubert problem. It is based on the geometric Littlewood-Richardson rule [20] and it is optimal in that generically there are no extraneous paths to be tracked.

We describe Schubert problems and their equations in §2, and give a detailed example of the geometric Littlewood-Richardson rule in §3. We then explain the local structure of the Littlewood-Richardson homotopy in §4. The next three sections give more details on the local coordinates, the moving flag, and the checker configurations. In §8 we discuss the global

---

2000 *Mathematics Subject Classification.* Primary 65H10. Secondary 14N15, 14Q99, 68W30.

*Key words and phrases.* continuation, geometric Littlewood-Richardson rule, Grassmannian, homotopies, numerical Schubert calculus, path following, polynomial system, Schubert problems.

Work of Sottile supported by the NSF under Grants DMS-0538734 and DMS-0915211.

Work of Vakil supported by the NSF under Grants DMS-0801196.

Work of Vershelde supported by the NSF under Grant No. 0713018.

structure of the Littlewood-Richardson homotopy and conclude in §9 with a brief description of our PHCpack [21] implementation and timings.

## 2. SCHUBERT PROBLEMS

A Schubert problem asks for the  $k$ -dimensional subspaces of  $\mathbb{C}^n$  that satisfy certain Schubert conditions imposed by general flags. We explain this in concrete terms.

A point in  $\mathbb{C}^n$  is represented by a  $n \times 1$  column vector and a linear subspace as the column span of a matrix. A flag  $F$  is represented by an ordered basis  $\mathbf{f}_1, \dots, \mathbf{f}_n$  of  $\mathbb{C}^n$  that forms the columns of a matrix  $F$ . If we write  $F_i$  for the span of the first  $i$  columns of  $F$ , then a Schubert condition imposed by  $F$  is the condition on the  $k$ -plane  $X$  that

$$(1) \quad \dim(X \cap F_{\omega_i}) \geq i \quad \text{for } 1 \leq i \leq k,$$

where  $\omega \in \mathbb{N}^k$  is a bracket;  $1 \leq \omega_1 < \omega_2 < \dots < \omega_k \leq n$ .

If we set  $|\omega| = \sum_i n - k + i - \omega_i$ , then a Schubert problem is a list  $\omega^1, \omega^2, \dots, \omega^s$  of brackets such that

$$(2) \quad |\omega^1| + |\omega^2| + \dots + |\omega^s| = k(n - k).$$

For example, the Schubert problem of three-planes meeting 12 four-planes in  $\mathbb{C}^7$  is given by 12 equal codimension one brackets and is written succinctly as  $[4 \ 6 \ 7]^{12}$ . The numerical condition (2) ensures that if  $F^1, \dots, F^s$  are general, then there are finitely many  $k$ -planes that satisfy condition  $\omega^i$  for flag  $F^i$ , for  $i = 1, \dots, s$ .

The set of  $k$ -planes  $X$  satisfying (1) is the Schubert variety  $\Omega_\omega(F)$ . This is a subvariety of the  $k(n-k)$ -dimensional Grassmannian of  $k$ -planes in  $n$ -space. Thus solving a Schubert problem corresponds to determining the intersection of Schubert varieties with respect to various flags.

These geometric conditions are formulated as systems of polynomials by parameterizing an appropriate subset of the Grassmannian. For example, for  $F \in \mathbb{C}^{6 \times 6}$ , the Schubert variety  $\Omega_{[2 \ 4 \ 6]}(F)$  contains

$$(3) \quad X = \begin{bmatrix} 1 & 0 & 0 \\ x_{21} & 1 & 0 \\ x_{31} & x_{32} & 1 \\ x_{41} & x_{42} & x_{43} \\ 0 & x_{52} & x_{53} \\ 0 & 0 & x_{63} \end{bmatrix} \quad \begin{array}{l} \dim(X \cap F_2) = 1 \\ \dim(X \cap F_4) = 2 \\ \dim(X \cap F_6) = 3 \end{array}$$

Expressed via conditions on the minors of  $[X|F_i]$  this is a system of 13 polynomials in 9 variables.

The most elementary Schubert problem involves only two brackets,  $\omega$  and  $\tau$  with  $|\omega| + |\tau| = k(n-k)$ . If  $F$  and  $M$  are general flags and  $\omega^\vee = [n+1-\omega_k \ \dots \ n+1-\omega_1]$ , then

$$(4) \quad \Omega_\omega(F) \cap \Omega_\tau(M) = \begin{cases} \langle \mathbf{x}_1, \dots, \mathbf{x}_k \rangle & \text{if } \tau = \omega^\vee, \\ \emptyset & \text{otherwise,} \end{cases}$$

where  $\mathbf{x}_i = F_{\omega_i} \cap M_{n+1-\omega_i}$ , which is one-dimensional and thus solved by linear algebra. Such elementary Schubert problems are the start systems for the Littlewood-Richardson homotopy.

When  $|\omega| + |\tau| < k(n-k)$ , an intersection

$$(5) \quad \Omega_\omega(F) \cap \Omega_\tau(M)$$

of Schubert varieties for general flags  $F$  and  $M$  has positive dimension. This intersection is homologous to a union of Schubert varieties  $\Omega_\sigma(F)$  for  $|\sigma| = |\omega| + |\tau|$ , each occurring with multiplicity the Littlewood-Richardson number  $c_{\omega,\tau}^\sigma$ . We write this formally as a sum,

$$(6) \quad \Omega_\omega(F) \cap \Omega_\tau(M) \sim \sum_{\sigma} c_{\omega,\tau}^\sigma \Omega_\sigma(F).$$

In the geometric Littlewood-Richardson rule [20], the flag  $M$  moves into special position with respect to the flag  $F$ . This changes the intersection (5), breaking it into components which are transformed into Schubert varieties  $\Omega_\sigma(F)$ . Then  $c_{\omega,\tau}^\sigma$  is the number of different ways to arrive at  $\Omega_\sigma(F)$ .

The relative position of the flags  $F$  and  $M$  is represented via a configuration of  $n$  black checkers in a  $n \times n$  board with no two in the same row or column. The dimension of  $M_a \cap F_b$  is the number of checkers weakly northwest of the square  $(a, b)$ . This is illustrated in Figure 1. Each cell corresponds to a vector space, and the vector space of each cell contains the vector

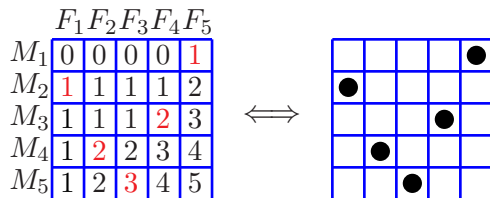


FIGURE 1. Dimension array  $\dim M_a \cap F_b$  and corresponding checker configuration.

spaces of the cells weakly northwest of it.

All components of the specializations of (5) are represented by placements of  $k$  red<sup>1</sup> checkers on a board with  $n$  checkers representing the relative positions of the flags. The red checkers represent the position of a typical  $k$ -plane in the component as follows: If the  $k$ -plane meets the vector space corresponding to a cell in dimension  $\ell$ , then there are  $\ell$  red checkers weakly northwest of it. See Figure 2 for examples. We discuss the placement and movement of the

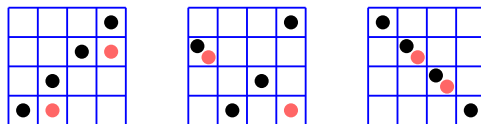


FIGURE 2. Three checkerboards with  $n = 4$  and  $k = 2$ .

checkers in §3 and §7.

Applying the geometric Littlewood-Richardson rule to two Schubert varieties in a Schubert problem of  $s$  brackets reduces it to Schubert problems involving  $s-1$  brackets. The Littlewood-Richardson homotopy begins with the solutions to those smaller problems and reverses the specializations to solve the original Schubert problem.

Let  $k = 3$  and  $n = 6$ , and consider this for the Schubert problem  $[2 \ 4 \ 6]^3 = [2 \ 4 \ 6][2 \ 4 \ 6][2 \ 4 \ 6]$ . Given three general flags  $F, M, N$ , we want to resolve the triple intersection

$$(7) \quad \Omega_{[2 \ 4 \ 6]}(F) \cap \Omega_{[2 \ 4 \ 6]}(M) \cap \Omega_{[2 \ 4 \ 6]}(N).$$

<sup>1</sup>Red checkers look grey when printed in black and white.

We first apply the geometric Littlewood-Richardson rule to the first intersection to obtain

$$(8) \quad (\Omega_{[2\ 3\ 4]}(F) + 2\Omega_{[1\ 3\ 5]}(F) + \Omega_{[1\ 2\ 6]}(F)) \cap \Omega_{[2\ 4\ 6]}(N),$$

and then apply (4) to obtain  $2\langle \mathbf{x}_1, \mathbf{x}_2, \mathbf{x}_3 \rangle$ , where  $\mathbf{x}_1 = F_1 \cap N_6$ ,  $\mathbf{x}_2 = F_3 \cap N_4$ , and  $\mathbf{x}_3 = F_5 \cap N_2$ .

The Littlewood-Richardson homotopy starts with the single 3-plane  $\langle \mathbf{x}_1, \mathbf{x}_2, \mathbf{x}_3 \rangle$  (counted twice) which is the unique solution to (8). It then numerically continues this solution backwards along the geometric specializations transforming (7) into (8) to arrive at solutions to (7). As the multiplicity 2 of  $\Omega_{[1\ 3\ 5]}(F)$  in (8) is the number of paths in the specialization that end in  $\Omega_{[1\ 3\ 5]}(F)$ , the single solution  $\langle \mathbf{x}_1, \mathbf{x}_2, \mathbf{x}_3 \rangle$  that we began with yields two solutions to (7).

### 3. THE PROBLEM OF FOUR LINES

We illustrate the Littlewood-Richardson homotopy via the classical problem of which lines in projective three-space ( $\mathbb{P}^3$ ) meet four given lines. This corresponds to two-planes in  $\mathbb{C}^4$  meeting four fixed two-planes nontrivially, or  $[2\ 4]^4$ .

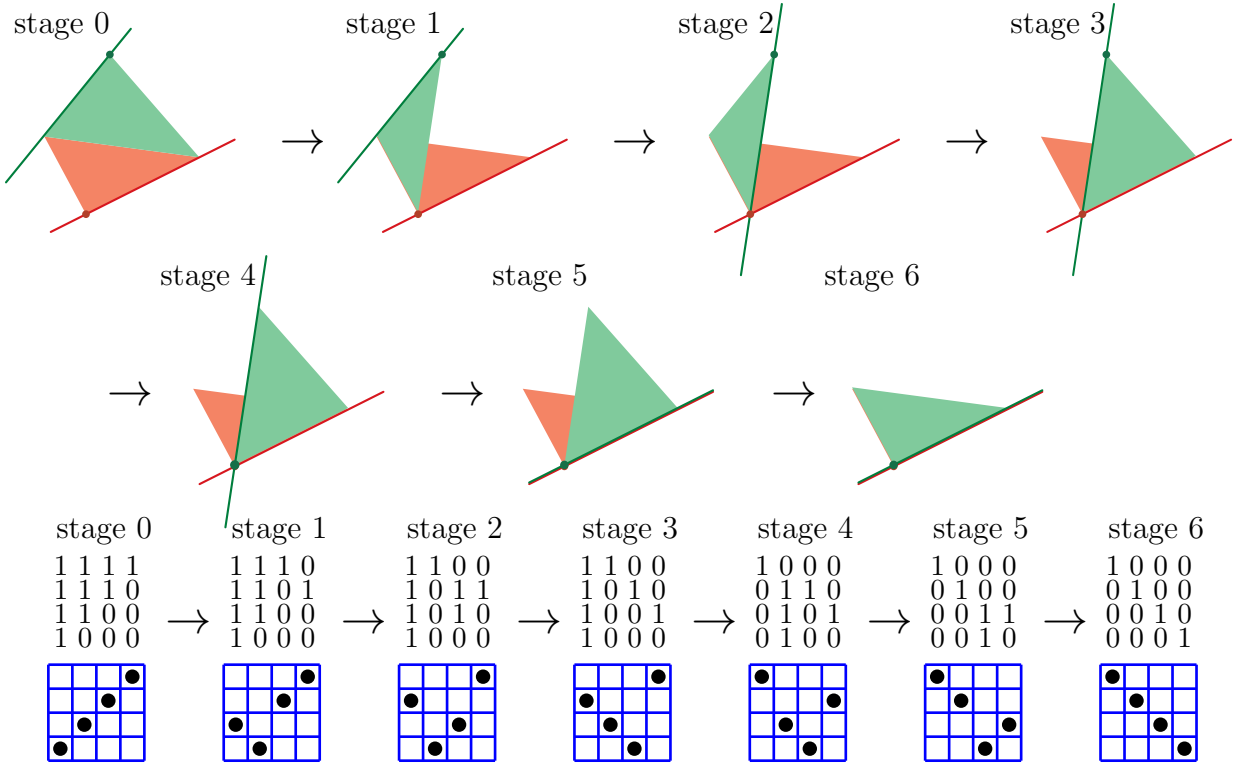


FIGURE 3. Specialization of the moving flag to the fixed flag.

A flag in  $\mathbb{P}^3$  consists of a point lying on a line that is contained in a plane (depicted here as a triangle). Figure 3 shows the specialization of two flags, one fixed and one moving, that underlies the geometric Littlewood-Richardson rule for every Schubert problem in  $\mathbb{P}^3$ . The top shows the geometry of the specialization. Below are matrices representing the moving flag and checkerboards representing the relative positions of the two flags. We recognize this as the bubble sort of the black checkers.

From stage 0 to stage 1 only the moving plane moves; the line and point are fixed. The plane moves until it contains the fixed point of the fixed flag. From stage 1 to stage 2 only the

moving line moves, until it too contains the fixed point. Then the moving plane moves again (to contain the fixed line); then the moving point; then the moving line; then the moving plane. At the end the two flags coincide.

We describe the solution to the problem of four lines using the Littlewood-Richardson homotopy. Let  $\ell_1, \ell_2, \ell_3, \ell_4$  be the four lines, where  $\ell_1$  is the line of the fixed flag,  $\ell_2$  the line of the moving flag, and  $\ell_3$  and  $\ell_4$  are two other general lines. The family of lines meeting  $\ell_1$  and  $\ell_2$  is two-dimensional; it is parameterized by  $\ell_1 \times \ell_2$ , as any line meeting  $\ell_1$  and  $\ell_2$  is determined by the points where it meets them. On this parameterized surface, we seek those points corresponding to lines satisfying the further condition (\*) of meeting  $\ell_3$  and  $\ell_4$ . Between stages 0 and 1, nothing changes, but in moving to stage 2,  $\ell_2$  moves to intersect  $\ell_1$ . There are now two distinct two-dimensional families of lines meeting both  $\ell_1$  and  $\ell_2$ : (a) those lines lying in the plane  $P$  containing  $\ell_1$  and  $\ell_2$  and (b) those lines in space passing through the point  $p = \ell_1 \cap \ell_2$ . We now impose the additional condition (\*) on both of these cases. In case (a),  $\ell_i$  meets  $P$  in a point  $p_i$  ( $i = 3, 4$ ), so there is one line in  $P$  meeting  $\ell_3$  and  $\ell_4$ , namely  $\overline{p_3 p_4}$ . In case (b), there is one line through  $p$  meeting  $\ell_3$  and  $\ell_4$ , namely  $\overline{p, \ell_3 \cap \ell_4}$ . After this, the only change is that the plane  $P$ , which equals the moving plane after stage 3, and rotates into the fixed plane between stages 5 and 6. To solve the original problem, we reverse this process, starting with the two solutions in cases (a) and (b), and reversing the specialization.

Note that we have reduced one problem involving 4 brackets to two problems involving 3 brackets.

Figure 4 shows the geometry and algebra behind this discussion. The top shows the geometry and the bottom gives the checker description. It also shows the matrices parameterizing the two-dimensional families of lines in each case. The parameterization is explicitly described in §5.

This single example is sufficient to understand the general case. The initial position of the red checkers is as follows. The intersection of the  $k$ -plane with the moving flag  $M$  determines the rows of the red checkers, and the intersection with the fixed flag  $F$  determines their columns, and they are arranged from southwest to northeast. The movement of the moving flag in arbitrary dimension is analogous to the specific case described here, and is described by a sequence of moves of black checkers. The movement of the black checkers determines the movement of the red checkers (see §7), and at each stage, there are one or two choices. When there are two choices, the underlying geometry is essentially the same as in the example above. When there is one choice, often the underlying geometry does not change, but the parameterization changes.

#### 4. THE LITTLEWOOD-RICHARDSON HOMOTOPY

We first explain how the geometric Littlewood-Richardson rule gives equations and homotopies for solving Schubert problems, and then illustrate that with two specific examples coming from the problem of four lines.

In the geometric Littlewood-Richardson rule the intersection  $\Omega_\omega(F) \cap \Omega_\tau(M)$  breaks into components which eventually become Schubert varieties  $\Omega_\sigma(F)$  as the moving flag  $M$  specializes to coincide with the fixed flag  $F$ . At each stage, the components correspond to checkerboards.

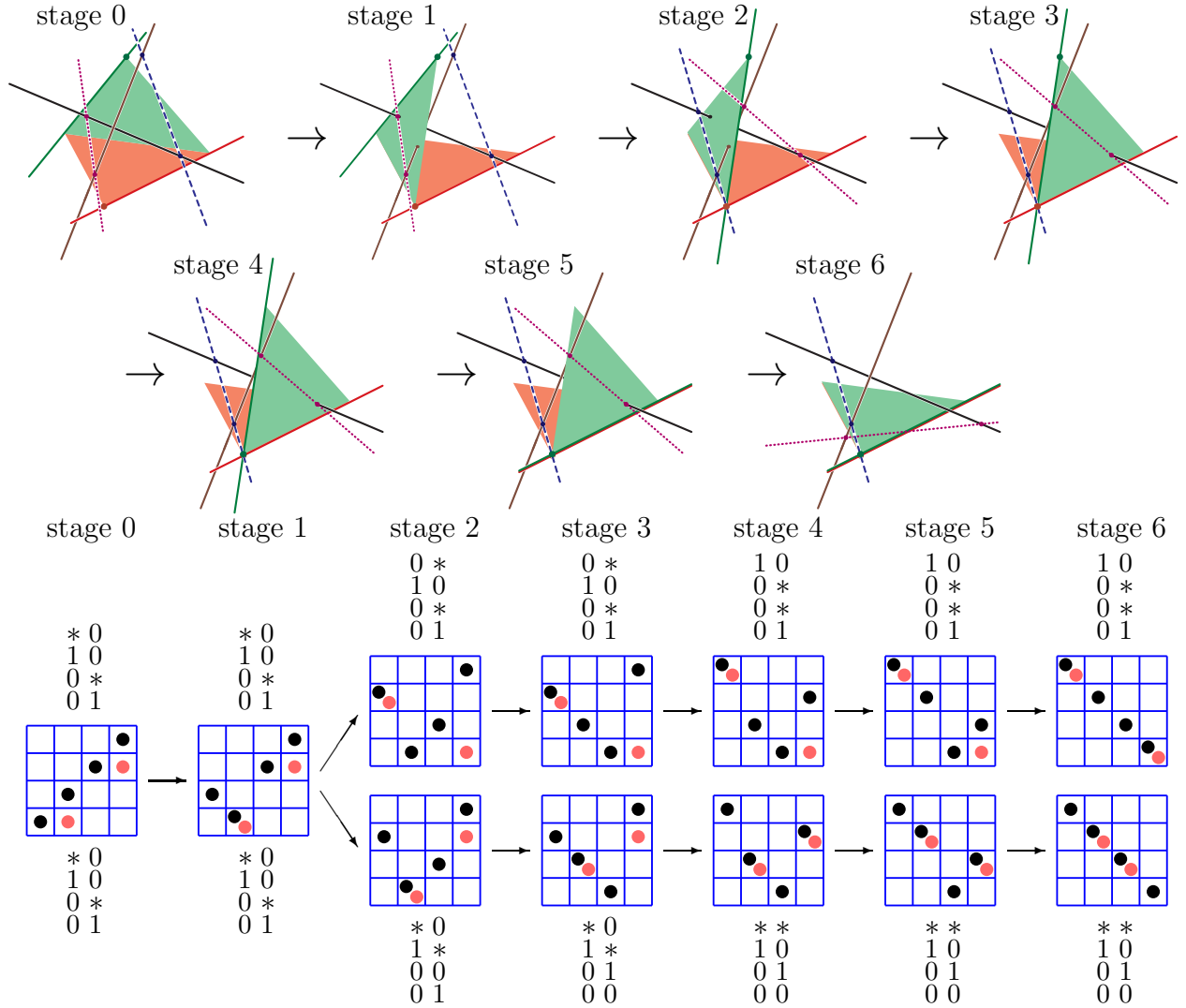


FIGURE 4. Resolving the problem of four lines.

A checkerboard encodes the relative positions of the fixed and moving flags as well as a representation  $X$ , called a localization pattern, of the general element in the corresponding component. Specifically,  $X$  is a  $n \times k$  matrix whose entries are either 0, 1, or indeterminates such that the  $n \times k$  matrix  $MX$  is a general point in that component. In §5 we explain how to obtain a localization pattern from its checkerboard.

Given a Schubert problem,

$$(9) \quad \Omega_\omega(F) \cap \Omega_\tau(M) \cap \Omega_{\rho_1}(N^1) \cap \cdots \cap \Omega_{\rho_s}(N^s),$$

the intersection of the last  $s$  Schubert varieties is expressed as rank conditions on (minors of) matrices  $[Y|N_j^s]$  (3), where  $Y$  is a general  $n \times k$  matrix representing a general  $k$ -plane. Write this system of minors succinctly as  $P(Y) = 0$ . When  $X$  is a localization pattern for a checkerboard in the degeneration of  $\Omega_\omega(F) \cap \Omega_\tau(M)$  (as in §5), the points in the corresponding

component that also lie in the last  $s$  Schubert varieties in (9) are the solutions to the system  $P(MX) = 0$ .

Reversing the specialization of the flags  $F$  and  $M$  is the generalization sequence. Between adjacent stages  $i$  and  $i+1$  of the generalization sequence, the moving flag is  $M(t)$  for  $t \in [0, 1]$ . Then the homotopy connecting these stages is

$$(10) \quad P(M(t)X) = 0$$

for  $t \in [0, 1]$ . When  $t = 0$ , we are in stage  $i$  and when  $t = 1$ , we are in stage  $i+1$ . The generalization of the moving flag is described in more detail in §6. We explain how the red checkers move in §7, and then how the localization patterns for different stages fit together.

We illustrate this with some examples from Figure 4. For  $X \in \Omega_{[2 \ 4]}(F) \cap \Omega_{[2 \ 4]}(M)$ , we have

$$(11) \quad X = \begin{bmatrix} x_{11} & 0 \\ 1 & 0 \\ 0 & x_{32} \\ 0 & 1 \end{bmatrix} \quad \begin{array}{l} F = [\mathbf{e}_1, \mathbf{e}_2, \mathbf{e}_3, \mathbf{e}_4] \\ M = [\mathbf{e}_4, \mathbf{e}_3, \mathbf{e}_2, \mathbf{e}_1] \\ \text{for any } x_{11} \text{ and } x_{32} : \\ \dim(X \cap \langle \mathbf{e}_1, \mathbf{e}_2 \rangle) = 1, \\ \dim(X \cap \langle \mathbf{e}_4, \mathbf{e}_3 \rangle) = 1, \\ \dim(X \cap \langle \mathbf{e}_1, \mathbf{e}_2, \mathbf{e}_3, \mathbf{e}_4 \rangle) = 2. \end{array}$$

In the first stage of Figure 4, the plane in the moving flag rotates about its line until it meets the fixed point. As the line in the moving flag does not move, there is no homotopy, only a change of coordinates, as illustrated in Figure 5 for a line meeting two lines and a

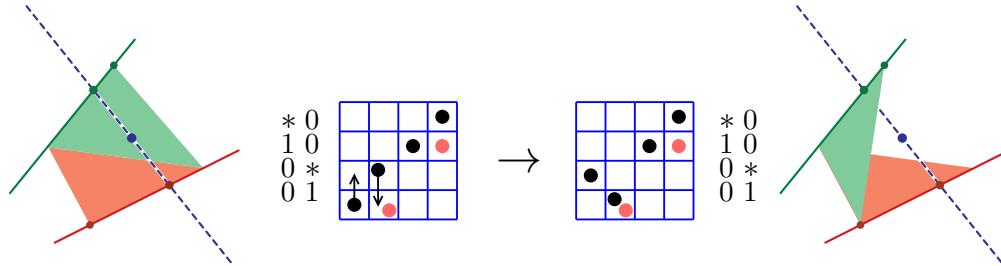


FIGURE 5. No homotopy, only change of coordinates.

fixed point in three-space, and as discussed at the end of §7. The corresponding coordinate transformation is:

$$(12) \quad \begin{bmatrix} 1 & 0 & 0 & 0 \\ 0 & 1 & 0 & 0 \\ 0 & 0 & 0 & 1 \\ 0 & 0 & 1 & -1 \end{bmatrix} \begin{bmatrix} x_{11} & 0 \\ 1 & 0 \\ 0 & x_{32} \\ 0 & 1 \end{bmatrix} = \begin{bmatrix} x_{11} & 0 \\ 1 & 0 \\ 0 & 1 \\ 0 & x_{32}-1 \end{bmatrix} \equiv \begin{bmatrix} x_{11} & 0 \\ 1 & 0 \\ 0 & 1/(x_{32}-1) \\ 0 & 1 \end{bmatrix}.$$

When the red checkers swap rows, we use a homotopy, shown in Figure 6, also for the case of a line meeting two lines and a fixed point. This homotopy has coordinates

$$(13) \quad X(t) = \begin{bmatrix} x_{12}t & x_{12} \\ x_{32} & 0 \\ x_{32}t & x_{32} \\ 0 & 1 \end{bmatrix}.$$

At  $t = 0$  we see that  $X(0)$  fits the pattern on the right in Figure 6, while at  $t = 1$  a coordinate change brings  $X(1)$  into the pattern on the left. With linear combinations of the two columns we find generators for the line that fit the columns of the pattern.

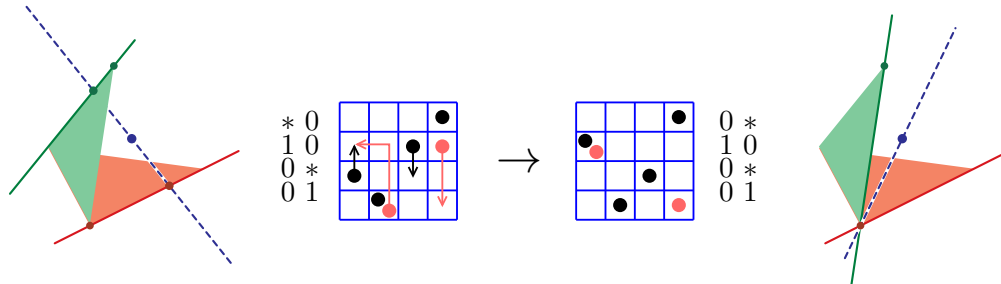


FIGURE 6. Homotopy, as red checkers swap rows.

## 5. LOCALIZATION PATTERNS

We describe coordinates for each component corresponding to a checkerboard: given two flags  $M$  and  $F$  in relative position described by the black checkers, it is the space of  $k$ -planes meeting  $M$  and  $F$  in the manner specified by the positions of the red checkers. The black checkers correspond to a basis of both  $F$  and  $M$ . Each red checker is a basis element for the  $k$ -plane and it lies in the space spanned by the black checkers weakly to its northwest.

While special cases were shown in Figure 4, we illustrate the general case with an example. In the checkerboard of Figure 7, one black checker (in row  $D$ ) is descending. Red checkers are distributed along the sorted black checkers (regions  $B$  and  $E$ ), as well as in the pre-sorted region (regions  $A$ ,  $C$ ,  $D$ , and  $F$ ); in the latter region, they are distributed from the southwest to the northeast as shown. The corresponding localization pattern, which is expressed with respect to the basis of  $M$ , is shown in Figure 7.

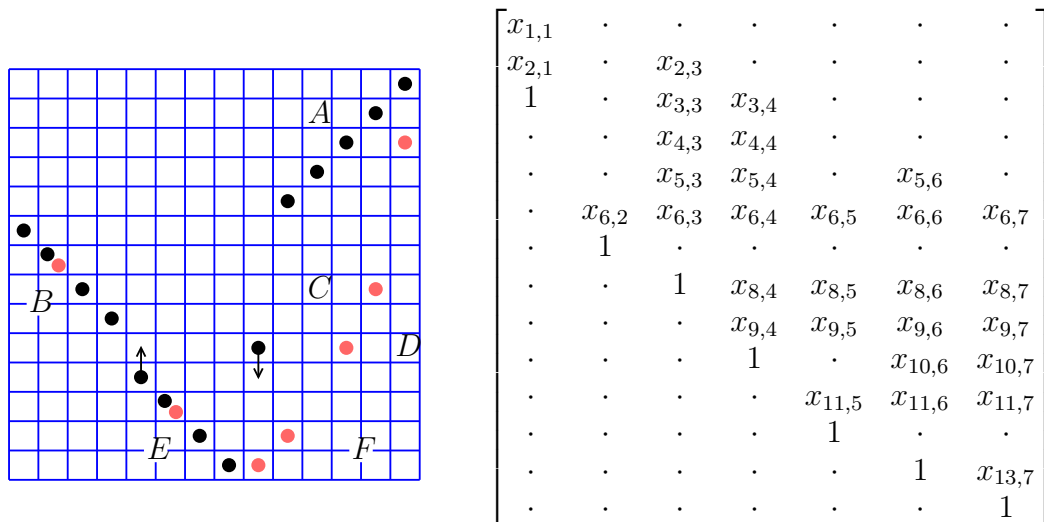


FIGURE 7. Coordinates corresponding to a checkerboard. Entries  $\cdot$  in the coordinate matrix are 0.



We discuss the linking of localization patterns between stages after we describe the movement of checkers in §7.

## 6. GENERALIZING THE MOVING FLAG

Underlying the geometric Littlewood-Richardson rule is the sequence of specializations (analogous to Figure 3) in which the moving flag  $M$  successively moves to coincide with the fixed flag  $F$ . Reversing this gives the generalization sequence in which  $M$  emerges from  $F$ .

The generalization of the moving flag  $M$  is as follows. Throughout, the fixed flag is

$$(14) \quad F = \{\langle \mathbf{e}_1 \rangle \subset \langle \mathbf{e}_1, \mathbf{e}_2 \rangle \subset \langle \mathbf{e}_1, \mathbf{e}_2, \mathbf{e}_3 \rangle \cdots\}.$$

Initially, the moving flag  $M$  coincides with  $F$ . We let  $\mathbf{m}'_i(t)$  describe the vectors during the generalization ( $t = 0$  corresponds to the specialized case, and  $t = 1$  corresponds to the generalized case), and  $\mathbf{m}''_i$  describe the vectors after the generalization. At time  $t$ ,

$$(15) \quad M(t) = \{\langle \mathbf{m}'_1(t) \rangle \subset \langle \mathbf{m}'_1(t), \mathbf{m}'_2(t) \rangle \subset \cdots\}.$$

In the checker diagram, at each stage the black checkers in rows  $r$  and  $r + 1$  swap rows, for some  $r$ . Set

$$(16) \quad \mathbf{m}_i = \mathbf{m}'_i(t) = \mathbf{m}''_i \quad \text{for } i \neq r, r + 1.$$

These different notations for the same vector keep track of whether we are talking about  $t = 0$ , general  $t$ , or  $t = 1$ .

$$(17) \quad \mathbf{m}_r = \mathbf{m}''_{r+1} (= \mathbf{m}'_r(0) = \mathbf{m}'_{r+1}(0)),$$

$$(18) \quad \mathbf{m}_{r+1} = \mathbf{m}''_{r+1} - \mathbf{m}''_r (= \mathbf{m}'_{r+1}(0) - \mathbf{m}'_r(0)).$$

$$(19) \quad \mathbf{m}'_r(t) = t\mathbf{m}''_r + (1 - t)\mathbf{m}''_{r+1} = \mathbf{m}''_{r+1} - t\mathbf{m}_{r+1},$$

$$(20) \quad \mathbf{m}'_i(t) = \mathbf{m}''_i \quad \text{for all other } i.$$

Thus  $\mathbf{m}'_i(1) = \mathbf{m}''_i$  for all  $i$ .

It is convenient to describe the homotopy in terms of matrices. Here are the generalizing moves from Figure 3.

$$(21) \quad F = \begin{bmatrix} 1 & 0 & 0 & 0 \\ 0 & 1 & 0 & 0 \\ 0 & 0 & 1 & 0 \\ 0 & 0 & 0 & 1 \end{bmatrix} \rightarrow \begin{bmatrix} 1 & 0 & 0 & 0 \\ 0 & 1 & 0 & 0 \\ 0 & 0 & \gamma_{31} & 1 \\ 0 & 0 & 1 & 0 \end{bmatrix} \rightarrow \begin{bmatrix} 1 & 0 & 0 & 0 \\ 0 & \gamma_{21} & 1 & 0 \\ 0 & \gamma_{31} & 0 & 1 \\ 0 & 1 & 0 & 0 \end{bmatrix} \rightarrow \begin{bmatrix} \gamma_{11} & 1 & 0 & 0 \\ \gamma_{21} & 0 & 1 & 0 \\ \gamma_{31} & 0 & 0 & 1 \\ 1 & 0 & 0 & 0 \end{bmatrix}$$

$$(22) \quad \rightarrow \begin{bmatrix} \gamma_{11} & 1 & 0 & 0 \\ \gamma_{21} & 0 & \gamma_{22} & 1 \\ \gamma_{31} & 0 & 1 & 0 \\ 1 & 0 & 0 & 0 \end{bmatrix} \rightarrow \begin{bmatrix} \gamma_{11} & \gamma_{12} & 1 & 0 \\ \gamma_{21} & \gamma_{22} & 0 & 1 \\ \gamma_{31} & 1 & 0 & 0 \\ 1 & 0 & 0 & 0 \end{bmatrix} \rightarrow \begin{bmatrix} \gamma_{11} & \gamma_{12} & \gamma_{13} & 1 \\ \gamma_{21} & \gamma_{22} & 1 & 0 \\ \gamma_{31} & 1 & 0 & 0 \\ 1 & 0 & 0 & 0 \end{bmatrix}.$$

Here,  $\gamma_{ij}$  are general complex numbers. For example, the second matrix in (22) corresponds to stage 1, and we see that the moving plane, (the projectivization of) the span of the first three columns, indeed contains the fixed point, as  $e_1$  is in the span of those three column vectors, in agreement with Figure 3.

The arrows represent the movement of the flag  $M$ , which we parametrize using our homotopy parameter  $t \in [0, 1]$ . For example, the next to last deformation is

$$(23) \quad \begin{bmatrix} \gamma_{11} & 1 & 0 & 0 \\ \gamma_{21} & 0 & \gamma_{22} & 1 \\ \gamma_{31} & 0 & 1 & 0 \\ 1 & 0 & 0 & 0 \end{bmatrix} \begin{bmatrix} 1 & 0 & 0 & 0 \\ 0 & \gamma_{12}t & 1 & 0 \\ 0 & 1 & 0 & 0 \\ 0 & 0 & 0 & 1 \end{bmatrix}$$

$$(24) \quad = \begin{bmatrix} \gamma_{11} & \gamma_{12}t & 1 & 0 \\ \gamma_{21} & \gamma_{22} & 0 & 1 \\ \gamma_{31} & 1 & 0 & 0 \\ 1 & 0 & 0 & 0 \end{bmatrix} =: M(t).$$

The gradual introduction of the random constants  $\gamma_{ij}$  in the moving flag is the analog here of the gamma trick [15] to ensure the regularity of the solution paths. By this gamma trick, for all  $t$ , except for a finite number of choices of  $\gamma_{ij}$ , the solution paths contain only regular points.

The Littlewood-Richardson homotopies operate on randomly generated complex flags. To move to flags with specific coordinates, we use coefficient-parameter [12] or cheater homotopies [10].

## 7. MOVEMENT OF RED CHECKERS

In the geometric Littlewood-Richardson rule, the black checkers start out on the anti-diagonal, and a bubble sort is performed which moves them to the diagonal. This is indicated in Figures 3, 4, and 7. In each of the  $\binom{n}{2}$  steps, one black checker descends and another rises as in Figure 8. The descending checker is in the critical row and the ascending checker is at

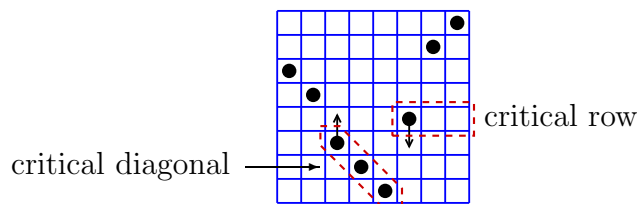


FIGURE 8. Critical row and critical diagonal.

the top left of the critical diagonal.

To resolve the intersection  $\Omega_\omega(F) \cap \Omega_\tau(M)$ , we initially place red checkers as follows. The intersection of the  $k$ -plane with the moving flag  $M$  determines the rows of the red checkers, and the intersection with the fixed flag  $F$  determines their columns, and they are arranged from southwest to northeast. As the black checkers move, they induce a motion of the red checkers. There will be nine cases to consider. In eight, the motion is determined, while in the ninth case there are sometimes two choices as in Figure 4.

The cases are determined by the answers to two questions, each of which has three answers.

- (1) Where is the top red checker in the critical diagonal?
  - (a) In the rising checker's square.
  - (b) Elsewhere in the critical diagonal.

- (c) There is no red checker in the critical diagonal.
- (2) Where is the red checker in the critical row?
  - ( $\alpha$ ) In the descending checker's square.
  - ( $\beta$ ) Elsewhere in the critical row.
  - ( $\gamma$ ) There is no red checker in the critical row.

Table 1 shows the movement of the checkers in these nine cases. The rows correspond to the answers to the first question and the columns to the answers of the second question. Only the relevant part of each checkerboard is shown.

	$\alpha$	$\beta$	$\gamma$
$a$			
$b$		 or 	
$c$			

TABLE 1. Movement of red checkers.

In case  $(b, \beta)$  there are two possibilities, which can both occur—this is when a component breaks into two components in the geometric Littlewood-Richardson rule. The second of these (where the red checkers swap rows) only occurs if there are no other red checkers in the rectangle between the two, which we call blockers. Figure 9 shows a blocker.

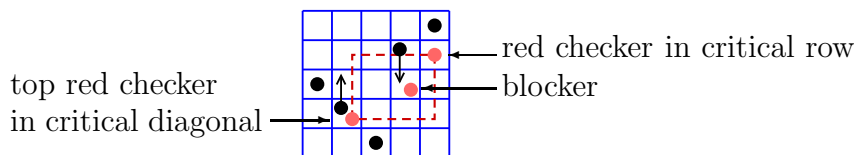


FIGURE 9. a blocker.

To track solutions to Schubert problems between adjacent stages in the generalization sequence, we need uniform coordinates corresponding to two adjacent diagrams—for example, two boards connected by an arrow in Figure 4. We can then track solutions from one board to the more generalized board. There are three cases to consider.

In trivial cases, such as the first arrow in Figure 4, which is case  $(c, \gamma)$  of Table 1, the coordinates do not change because the underlying geometry is constant.

We describe one of the nontrivial examples of the coordinates linking two stages, that of the lower arrow between stage 1 and stage 2 in Figure 4 (left case of  $(b, \beta)$ ). We follow the vector corresponding to the red checker in the bottom row. Throughout the degeneration (as  $t$  goes from 0 to 1), we write its vector as  $\mathbf{m}_4 + x\mathbf{m}'_2(t)$ . As  $\mathbf{m}'_2(1) = \mathbf{m}''_2$  and  $\mathbf{m}'_2(0) = \mathbf{m}''_3$

(see (17)–(20) of §6 with  $r = 2$ ), we see that the reason for the change of row of the  $*$  in the matrix in Figure 4 is just a renaming of the variable.

The third case, where the two red checkers swap rows, is more subtle, and an example was described at the end of §4.

## 8. SOLVING SCHUBERT PROBLEMS

The global structure of the Littlewood-Richardson homotopy is encoded by a graded poset. This records the branching of Schubert varieties that occur in when running the geometric Littlewood-Richardson rule through successive specializations of their defining flags, equivalently, moving checkers as in §7.

We construct the poset for a a Schubert problem

$$(25) \quad \Omega_{\omega^1}(F^1) \cap \Omega_{\omega^2}(F^2) \cap \cdots \cap \Omega_{\omega^s}(F^s).$$

First, use the geometric Littlewood-Richardson rule to resolve the first intersection

$$(26) \quad \Omega_{\omega^1}(F^1) \cap \Omega_{\omega^2}(F^2) \sim \sum_{\sigma} c_{\omega^1, \omega^2}^{\sigma} \Omega_{\sigma}(F^1).$$

The top of the poset is the bracket  $\omega^1$ , which branches to those brackets  $\sigma$  appearing in the sum. The edge  $\omega^1 \rightarrow \sigma$  occurs with multiplicity  $c_{\omega^1, \omega^2}^{\sigma}$ . Geometrically, we have the disjunction of Schubert problems

$$(27) \quad \left( \sum_{\sigma} c_{\omega^1, \omega^2}^{\sigma} \Omega_{\sigma}(F^1) \right) \cap \Omega_{\omega^3}(F^3) \cap \cdots \cap \Omega_{\omega^s}(F^s),$$

and we resolve each  $\Omega_{\sigma}(F^1) \cap \Omega_{\omega^3}(F^3)$  with the geometric Littlewood-Richardson rule, further building the poset, and continue in this fashion.

The penultimate stage has the form

$$(28) \quad \left( \sum_{\sigma} C^{\sigma} \Omega_{\sigma}(F^1) \right) \cap \Omega_{\omega^s}(F^s),$$

where  $C^{\sigma}$  are the multiplicities. This is resolved via (4), so the only term in the sum which contributes is when  $\sigma^{\vee} = \omega^s$ , and the final Schubert variety is  $\Omega_{[1 \ 2 \ \dots \ k]}(F^1)$ .

The global structure of the Littlewood-Richardson homotopy is to begin with the solution  $\Omega_{[1 \ 2 \ \dots \ k]}(F^1)$  at the bottom of our poset, and continue this solution along homotopies corresponding to the edges of the poset. Each edge is a sequence of  $\binom{n}{2}$  homotopies or coordinate changes corresponding to running the geometric Littlewood-Richardson rule backwards, as explained in §5, §6, and §7. In this way, we iteratively build solutions to the Schubert-type problems corresponding to the nodes of this poset.

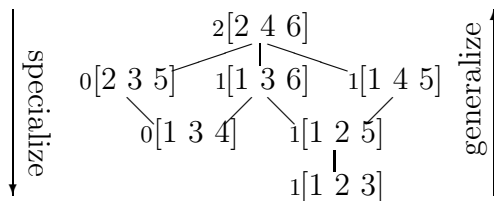
For example, suppose that we have the Schubert problem  $[2 \ 4 \ 6][2 \ 5 \ 6]^3$ . This is resolved in the geometric Littlewood-Richardson rule as

$$(29) \quad [2 \ 4 \ 6][2 \ 5 \ 6]^3 = (1[2 \ 3 \ 5] + 1[1 \ 4 \ 5] + 1[1 \ 3 \ 6])[2 \ 5 \ 6]^2$$

$$(30) \quad = (2[1 \ 3 \ 4] + 2[1 \ 2 \ 5])[2 \ 5 \ 6]$$

$$(31) \quad = 2[1 \ 2 \ 3].$$

The poset corresponding to the Littlewood-Richardson homotopies is shown in Figure 10. The multiplicities in front of the brackets are the number of solutions tracked to the given Schubert variety.

FIGURE 10. Poset to resolve  $[2\ 4\ 6][2\ 5\ 6]^3$ .

The number of solution paths is one of the three factors that determine the cost of the homotopies. Another factor is the complexity of the polynomials that express the intersection conditions. The current implementation performs a Laplace expansion on the minors to elaborate all conditions (1). Locally, for use during path following, an overdetermined system of  $p$  equations in  $q$  unknowns is multiplied with a  $q$ -by- $p$  matrix of randomly generated complex coefficients to obtain square linear systems in the application of Newton's method. The third factor in the cost lies in the complex and real geometry of the solution paths. In practice it turns out that solving a generic complex instance with the Pieri homotopies is in general always faster than running a cheater homotopy using the solutions of a generic complex instance as start solutions to solve a generic real instance. This experience also applies to solving general Schubert problems with Littlewood-Richardson homotopies.

## 9. COMPUTATIONAL EXPERIMENTS

Littlewood-Richardson homotopies are available in PHCpack [21] since release 2.3.46. Release 2.3.52 contains `LRhomotopies.m2`, an interface to solve Schubert problems in Macaulay 2 [5]. Via `phc -e option #4` we resolve intersection conditions and Littlewood-Richardson homotopies are available via option #5.

Below we list sample timings for solving some small Schubert problems on one core of a Mac OS X 2.2 Ghz:

- $[2\ 4]^4 = 2$  takes 5 milliseconds,
- $[2\ 4\ 6]^3 = 2$  takes 169 milliseconds,
- $[2\ 5\ 8]^2[4\ 6\ 8] = 2$  takes 2.556 seconds,
- $[2\ 4\ 6\ 8]^2[2\ 5\ 7\ 8] = 3$  takes 8.595 seconds.

## REFERENCES

- [1] R.W. Brockett and C.I. Byrnes. Multivariate Nyquist criteria, root loci, and pole placement: a geometric viewpoint. *IEEE Trans. Automat. Control*, 26(1):271–284, 1981.
- [2] C.I. Byrnes. Pole assignment by output feedback. In H. Nijmacker and J.M. Schumacher, editors, *Three Decades of Mathematical Systems Theory*, volume 135 of *Lecture Notes in Control and Inform. Sci.*, pages 13–78. Springer-Verlag, 1989.
- [3] A. Eremenko and A. Gabrielov. Pole placement by static output feedback for generic linear systems. *SIAM J. Control Optim.*, 41(1):303–312, 2002.
- [4] W. Fulton. *Young Tableau. With Applications to Representation Theory and Geometry*. Cambridge University Press, 1997.
- [5] D.R. Grayson and M.E. Stillman. Macaulay 2, a software system for research in algebraic geometry. Available at <http://www.math.uiuc.edu/Macaulay2/>.
- [6] C. Hillar, L. Garcia-Puente, A. Martin del Campo, J. Ruffo, Z. Teitler, S.L. Johnson, and F. Sottile. Experimentation at the frontiers of reality in Schubert calculus. Preprint [arXiv:0906.2497v2](https://arxiv.org/abs/0906.2497v2) [math.AG].

- [7] B. Huber, F. Sottile, and B. Sturmfels. Numerical Schubert calculus. *J. Symbolic Computation*, 26(6):767–788, 1998.
- [8] B. Huber and J. Verschelde. Pieri homotopies for problems in enumerative geometry applied to pole placement in linear systems control. *SIAM J. Control Optim.*, 38(4):1265–1287, 2000.
- [9] A. Leykin and F. Sottile. Galois group of schubert problems via homotopy continuation. *Math. Comp.*, 78(267):1749–1765, 2009.
- [10] T.Y. Li, T. Sauer, and J.A. Yorke. The cheater’s homotopy: an efficient procedure for solving systems of polynomial equations. *SIAM J. Numer. Anal.*, 26(5):1241–1251, 1989.
- [11] T.Y. Li, X. Wang, and M. Wu. Numerical Schubert calculus by the Pieri homotopy algorithm. *SIAM J. Numer. Anal.*, 20(2):578–600, 2002.
- [12] A.P. Morgan and A.J. Sommese. Coefficient-parameter polynomial continuation. *Appl. Math. Comput.*, 29(2):123–160, 1989. Errata: *Appl. Math. Comput.* 51:207(1992).
- [13] M.S. Ravi, J. Rosenthal, and X. Wang. Dynamic pole placement assignment and Schubert calculus. *SIAM J. Control and Optimization*, 34(3):813–832, 1996.
- [14] H. Schubert. Anzahl-Bestimmungen für lineare Räume beliebiger Dimension. *Acta Math.*, 8:97–118, 1886.
- [15] A.J. Sommese and C.W. Wampler. *The Numerical solution of systems of polynomials arising in engineering and science*. World Scientific, 2005.
- [16] F. Sottile. Enumerative real algebraic geometry. In S. Basu and L. Gonzalez-Vega, editors, *Algorithmic and Quantitative Real Algebraic Geometry*, pages 139–180. AMS, 2003.
- [17] F. Sottile. Frontiers of reality in Schubert calculus. *Bulletin of the AMS*, 47(1):31–71, 2010.
- [18] Frank Sottile. Pieri’s formula via explicit rational equivalence. *Canad. J. Math.*, 49(6):1281–1298, 1997.
- [19] Frank Sottile. Real Schubert calculus: polynomial systems and a conjecture of Shapiro and Shapiro. *Experiment. Math.*, 9(2):161–182, 2000.
- [20] R. Vakil. A geometric Littlewood-Richardson rule. *Annals of Math.*, 164(2):376–421, 2006.
- [21] J. Verschelde. Algorithm 795: PHCpack: A general-purpose solver for polynomial systems by homotopy continuation. *ACM Trans. Math. Softw.*, 25(2):251–276, 1999. Software available at <http://www.math.uic.edu/~jan>.
- [22] J. Verschelde. Numerical evidence for a conjecture in real algebraic geometry. *Experimental Mathematics*, 9(2):183–196, 2000.
- [23] J. Verschelde and Y. Wang. Computing dynamic output feedback laws. *IEEE Trans. Automat. Control.*, 49(8):1393–1397, 2004.
- [24] J. Verschelde and Y. Wang. Computing feedback laws for linear systems with a parallel Pieri homotopy. In Y. Yang, editor, *Proceedings of the 2004 International Conference on Parallel Processing Workshops, 15-18 August 2004, Montreal, Quebec, Canada. High Performance Scientific and Engineering Computing*, pages 222–229. IEEE Computer Society, 2004.

(Sottile) DEPARTMENT OF MATHEMATICS, TEXAS A&M UNIVERSITY, COLLEGE STATION, TX 77843  
*E-mail address:* [sottile@math.tamu.edu](mailto:sottile@math.tamu.edu)  
*URL:* <http://www.math.tamu.edu/~sottile/>

(Vakil) DEPARTMENT OF MATHEMATICS, STANFORD UNIVERSITY, STANFORD, CA 94305  
*E-mail address:* [vakil@math.stanford.edu](mailto:vakil@math.stanford.edu)  
*URL:* <http://math.stanford.edu/~vakil>

(Verschelde) DEPARTMENT OF MATHEMATICS, STATISTICS, AND COMPUTER SCIENCE, UNIVERSITY OF ILLINOIS AT CHICAGO, 851 SOUTH MORGAN (M/C 249), CHICAGO, IL 60607-7045  
*E-mail address:* [jan@math.uic.edu](mailto:jan@math.uic.edu)  
*URL:* <http://www.math.uic.edu/~jan>

